analytical chemistry

pubs.acs.org/ac Article

# A SERS-Active Electrospun Polymer Mesh for Spatially Localized pH Measurements of the Cellular Microenvironment

William H. Skinner,[#] Michael Chung,[#] Stephen Mitchell, Asli Akidil, Kristin Fabre, Richard Goodwin, Adam A. Stokes, Norbert Radacsi, and Colin J. Campbell*

Cite This: *Anal. Chem.* 2021, 93, 13844−13851 Read Online

ACCESS | Metrics & More | Article Recommendations | Supporting Information

**ABSTRACT:** Extracellular pH (pHe) is an important chemical factor in many cellular processes and disease pathologies. The routine sampling of pHe *in vitro* could lead to innovative advances in therapeutics. To this end, we have fabricated a novel gold-coated polymer mesh, which facilitates the real-time measurement of pHe via surface-enhanced Raman scattering (SERS). In this proof of concept study, we apply our SERS sensor to measure metabolically induced changes in the pHe of carcinoma-derived cell line HepG2/C3A. We demonstrate that gold-coated polyurethane electrospun nanofibers (AuNF) have strong and reproducible SERS spectra of surface-adsorbed analytes. By functionalizing AuNF with pH-responsive reporter 4-mercaptobenzoic acid (MBA), we have developed an accurate pH SERS sensor for the extracellular microenvironment. We cultured HepG2/C3A on the surface of MBA-AuNF and measured an acidic shift in pHe at the cell−fiber interface. Following exposure to staurosporine, an apoptosis-inducing drug, we observed changes in the HepG2/C3A cellular morphology indicative of controlled cell death, and detected an increase in the pHe of HepG2/C3A. These results demonstrate how subtle changes in pHe, induced by the metabolic activity of cells, can be measured with our novel SERS sensor MBA-AuNF. The excellent pH measurement performance of MBA-AuNF provides a unique platform to study extracellular pH on the microscale and will help to deepen our understanding of pHe in disease pathology.

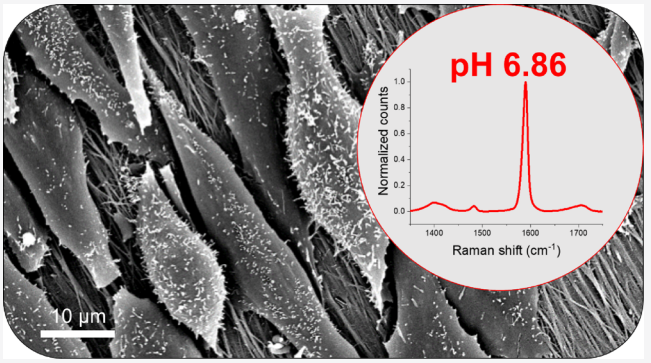


The extracellular pH (pHe) of tissue is a key regulating factor in the physiological activity of cells.[1] Aberrant pHe in the cellular microenvironment is implicated in the progression of diseases such as cancer and cystic fibrosis.[2−4] However, the pHe of the cellular microenvironments *in vitro* is challenging to measure because of the microscale of the sensing target and the spatial targeting requirements of the sensor. To this end, there is a need to develop a facile means to measure the pHe of cell cultures *in vitro*.

The sensing methods used to measure pH *in vivo* are not easily applied to *in vitro* cell culture. Magnetic resonance imaging (MRI) is used to measure pHe in tissue but has limited spatial resolution and is not suitable for the high throughput analysis required for *in vitro* cell cultures.[5] The use of pH electrodes to measure pHe *in vitro* is also limited due to the technical feasibility of positioning the probe in the cellular microenvironment.

Fluorescence-based pH-sensitive molecular probes are a well-established means of measuring intracellular pH *in vitro*. However, to measure pHe, these molecular probes must be retained on the cell surface, without being internalized by the cell or diffusing away.[6] Cell-surface-anchored probes, employing low pH insertion peptides and streptavidin−biotin interactions, have been developed to overcome this challenge.[7,8] These approaches are limited because their application is complex, and the probe-cell anchors have the potential to disrupt cell physiology and induce adverse biological responses.[6]

Recently, plasmonic nanostructured cell culture platforms have been developed to measure pHe using surface-enhanced Raman spectroscopy (SERS).[9,10] Raman spectroscopy is a rapid, non-invasive spectroscopic technique that enables fingerprinting of biological and chemical samples. SERS enhances the intensity of the Raman fingerprint of molecules in proximity to plasmonic nanostructures[11] and has several advantages over fluorescence, including multiplexed detection, low autofluorescence, and resistance to photobleaching.[12,13] Furthermore, SERS requires the molecular probe to be anchored to a solid phase plasmonic substrate. If the size of this substrate is designed to be too large for the cells to

**Received:** June 16, 2021
**Accepted:** September 22, 2021
**Published:** October 5, 2021







https://doi.org/10.1021/acs.analchem.1c02530
*Anal. Chem.* 2021, 93, 13844−13851

endocytose, the sensor will be restricted to the extracellular space with no risk of cell internalization. These characteristics make SERS-active cell culture platforms excellent candidates for non-invasive *in situ* pHe monitoring of the cellular microenvironment.

SERS substrates for pHe sensing have been fabricated with electron-beam lithography and metallic nanoparticle assemblies.[9,10] Functionalizing these plasmonic substrates with pH-sensitive Raman reporter molecules 4-mercaptobenzoic acid (MBA) or mercaptopyridine (MPY) facilitates pH measurements at the substrate surface with Raman spectroscopy. pHe SERS substrates have been used to support *in vitro* cell cultures and distinguish differences in local pHe between tumor cell lines and normal cell lines.[9,10]

In this paper, we present a novel SERS active substrate, gold-coated polyurethane electrospun nanofibers (AuNF) and apply it to measure the pHe of *in vitro* cell cultures. We fabricate polyurethane nanofibers using a "benchtop" process called electrospinning. By sputter coating the fibers with gold, we leverage the inherent nanoscale architecture of the fibers to create a plasmonic substrate, AuNF, for SERS pHe sensing.[14] This two-step fabrication process is low cost and does not require specialist photolithographic technologies, or colloidal nanoparticles, which are typically used to create SERS substrates for pHe sensing.[9,15,16] Furthermore, the advent of high-throughput electrospinning, and the low cost and simplicity of the process we document, makes AuNF a pHe SERS substrate well suited to fabricate at scale.[17]

In a conventional electrospinning setup, a polymer solution is loaded into a syringe and a large potential difference is applied between the syringe and a target (Scheme 1). When

**Scheme 1. Electrospinning Apparatus**

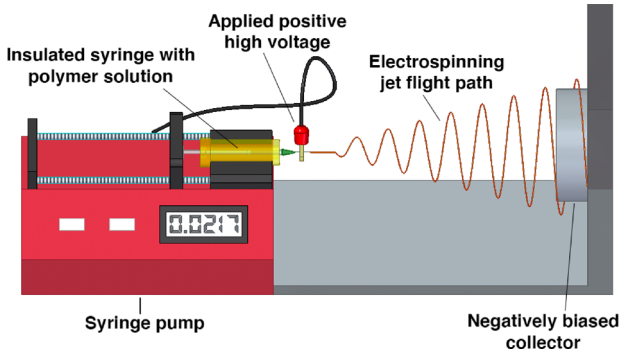


the surface tension barrier of the polymer solution is overcome, a thin jet of solution spirals toward the negatively biased collector.[14] The solvent evaporates during this flight, and dry polymer fibers are collected on the target. These electrospun polymer fibers have high surface-volume ratios and controllable material properties, which make them suitable for applications in sensing, cell culture, and wound healing scaffolds.[18,19] Extracellular matrices for a range of tissues have been developed by controlling fiber thickness and mesh density.[19−21]

A widely used method of creating SERS substrates from electrospun nanofibers is to decorate the fibers with metallic nanoparticles.[16,22] We demonstrate that in the absence of nanoparticles, gold-coated polyurethane nanofibers yield a strong SERS enhancement suitable for *in situ* pH sensing. This simplifies the substrate fabrication process, removing the need for technically challenging nanoparticle synthesis and removing the risk of nanoparticle leaching. Nanoparticle leaching could lead to endocytosis and the inadvertent measurement of intracellular pH instead of pHe.[23]

In this study, we functionalized AuNF with MBA (MBA-AuNF) and created a SERS-active cell culture platform that could monitor pHe in the cellular microenvironment. MBA-AuNF had excellent pH sensitivity between pH 6 and 8, which was spatially consistent over the fiber substrate. To demonstrate the biomedical sensing application of MBA-AuNF, we cultured HepG2/C3A cells on the fiber surface and measured an acidic pHe at the cell−fiber interface. We then treated the HepG2/C3A cells with nonspecific protein kinase inhibitor staurosporine (STS) and measured an increase in local pHe simultaneous to changes in the cell morphology, which are associated with apoptosis. This demonstrates the potential of MBA-AuNF as a tool to investigate the relationship between intracellular processes and pHe.

## EXPERIMENTAL SECTION

**AuNF Fabrication.** We used polydimethylsiloxane (PDMS) as a flexible and transparent support to electrospin polyurethane fibers onto. We prepared the PDMS (Sylgard 184) by adding the catalyst to the base reagent at a weight ratio of 1:10. We poured this mixture into a mold to a depth of 0.5 mm and cured it for 1 h at 100 °C. We then cut the PDMS into sheets of 30 × 60 mm, into which rows of 6 mm holes were cut at 1 cm intervals using a biopsy punch. This allowed access to the negatively biased electrospinner collector through the electrically insulating PDMS film and facilitated the collection of fibers on the surface of the PDMS between the holes (Figure S1).

We prepared 10 mL of electrospinning solution by adding 1.8 g of thermoplastic polyurethane (TPU) to 8.2 mL of dimethylformamide (DMF). The TPU solution was mixed with a magnetic stirrer for 24 h at an RPM of 200, at 80 °C, after which we added 50 μL of 37% hydrochloric acid to the TPU solution. We used a horizontal needle electrospinning setup (IME Medical Electrospinning, Netherlands) to fabricate the fibers. The TPU solution was added to a 1 mL syringe with a 21G (0.8 mm diameter) blunt needle and placed in a syringe pump set at a flow rate of 5 $\mu L \cdot min^{-1}$. The PDMS sheet, described above, was placed on the metallic collector set at a distance of 20 cm away from the needle tip. We applied a positive voltage of 20 kV to the needle and biased the collector to −4 kV. During electrospinning, the ambient temperature was 20−23 °C and the relative humidity was between 30 and 40%. We electrospun the TPU onto the PDMS for 5 min to obtain an ultrathin layer of polyurethane fibers on the PDMS surface (Figure S1). The fibers, supported by PDMS, were coated with 30 nm of gold using an automatic sputter coater (Agar Scientific Ltd., UK) with a 57 mm diameter gold target. We checked the fiber morphology using a JSM-IT100 scanning electron microscope (SEM) (JEOL Ltd., Japan). Mean fiber diameter was calculated using ImageJ software by taking 50 diameter measurements from two separate 2000× magnification SEM images.

Following the application of the gold layer, we cut the PDMS-mounted fiber samples (AuNF) into 2.5 × 2.5 mm squares with a surgical scalpel.

**Biocompatibility of AuNF.** We incubated AuNF in a solution of collagen (100 μg/mL) in phosphate buffer solution (PBS) (NaCl 137 mM, KCl 2.7 mM, $Na_2HPO_4$ 10 mM,


https://doi.org/10.1021/acs.analchem.1c02530
Anal. Chem. 2021, 93, 13844−13851

$KH_2PO_4$ 1.8 mM) for 2 h at 37 °C and then seeded HepG2/C3A cells onto the AuNF at $3.1 \times 10^4$ cells/cm$^2$. We measured the relative increase in the number of viable cells between 20 and 63 h after seeding with an ATP assay CellTiter-Glo (Promega). Luminescence was measured using a SpectraMax M5 plate reader (Molecular Devices) and an exposure time of 0.5 s.

**AuNF Surface Modification.** We immersed the AuNF in a 100 $\mu$M solution of MBA in 1% ethanol (EtOH) in deionized water (DI) and incubated it for 24 h at 8 °C. The following day, we washed the MBA-AuNF with ×1 70% EtOH in DI and ×2 PBS.

**MBA-AuNF pH Calibration.** We calibrated the MBA-AuNF pH sensors by collecting SERS spectra from the fiber surface at pH 5−8. We used Specpure buffers for pH 5, 6, 7, and 8, and phosphate-buffered saline solution for pH 7.2 and 7.4. For each pH in the calibration curve, we collected nine SERS spectra (Figure S2), from three random areas, on three MBA-AuNF substrates. All spectra were collected using the Renishaw InVia Raman spectroscope, with a 60×/N.A. = 1 water immersion objective and 785 nm laser. For spectral acquisitions, we used a 0.5 mW laser power and 2 s acquisition time. We processed all spectra with 9-point Savitsky-Golay smoothing (polynomial order 3) and baseline subtraction with the WiRe intelligent fitting function. We calculated the intensity ratio of the MBA carboxylic acid peak ($\nu_s$(COO)) at ∼1400 cm$^{-1}$ and the ring deformation mode ($\nu$(ref)) at ∼1590 cm$^{-1}$ for each spectrum using a bespoke MatLab code. Origin was used to plot the calibration data and fit a Boltzmann curve.

We validated our MBA-AuNF pH calibration curve by collecting Raman maps from MBA-AuNF in buffers at pH 6, 7, 7.4, and 8 and calculating pH from the spectra. We collected Raman spectra at 10 $\mu$m intervals in a 80 × 90 $\mu$m area on the MBA-AuNF surface, with the same Raman microscope settings used for pH calibration. We used the pH calibration curve to calculate pH from the intensity ratio of $\nu_s$(COO) and $\nu$(ref) in each MBA-AuNF spectrum.

**Cell Culture on MBA-AuNF.** We cultured HepG2/C3A up to passage 10 in collagen-coated flasks in Dulbecco's modified eagle medium (DMEM) and high glucose, with 10% fetal bovine serum and 1% penicillin−streptomycin.

We prepared MBA-AuNF for cell culture by sterilizing the fibers with 70% EtOH in DI and washing ×2 with PBS. The MBA-AuNF were then incubated in a solution of 100 $\mu$g/mL of collagen (type 1) in PBS for 2 h at 37 °C, following which, we seeded HepG2/C3A, at $2 \times 10^5$ cells/cm$^2$, onto the MBA-AuNF. We cultured the cells on MBA-AuNF for 24 h at 37 °C and 5% $CO_2$ before collecting pHe measurements.

**Cell Fixing for SEM.** We fixed HepG2/C3A cultures, on MBA-AuNF, in a solution of 3% glutaraldehyde in 0.1 M sodium cacodylate buffer (pH 7.3) for 2 h. The cells were then washed in 3 × 10 min changes of 0.1 M sodium cacodylate buffer. We postfixed the samples in 1% osmium tetroxide in 0.1 M sodium cacodylate buffer for 45 min. We then performed 3 × 10min washes of the sample in 0.1 M sodium cacodylate buffer. We dehydrated the cells in graded concentrations of acetone (50, 70, 90, and 3 × 100%) for 10 min each followed by critical point drying using liquid carbon dioxide. We mounted the samples on aluminum stubs for sputter coating with 20 nm gold and imaged the cells using a JSM-IT100 scanning electron microscope (SEM) (JEOL Ltd., Japan).

**HepG2/C3A pHe Measurements.** We analyzed MBA-AuNF 24 h after cell seeding, at which point a confluent layer of HepG2/C3A had formed on the MBA-AuNF surface. For spectral acquisition, the cells were washed (×1) and submerged in a PBS imaging solution (NaCl 137 mM, KCl 2.7 mM, $Na_2HPO_4$ 1 mM, $KH_2PO_4$ 0.18 mM). We collected spectra from each sample for a maximum of 10 min, using the same microscope and laser settings we used for MBA-AuNF pH calibration. We collected nine MBA SERS spectra (Figure S3) from three 100 × 150 $\mu$m areas on three MBA-AuNF with confluent layers of HepG2/C3A. We used the pH calibration curve to calculate pH from the intensity ratio of $\nu_s$(COO) and $\nu$(ref) in each MBA-AuNF spectrum.

**pHe Measurements after Staurosporine Exposure.** HepG2/C3A were seeded onto MBA-AuNF as previously described. After cell seeding for 24 h, we treated three MBA-AuNF cell cultures with 1 $\mu$M of staurosporine (STS) in a solution of 0.01% dimethyl sulfoxide (DMSO) in DMEM. As a vehicle control, we treated three MBA-AuNF cell cultures with a solution of 0.01% DMSO in DMEM. Following 3 h of incubation, we washed (×1) and submerged the cultures in PBS imaging solution for spectral acquisition. We collected spectra from each sample for a maximum of 10 min, using the same microscope and laser settings that we used for MBA-AuNF pH calibration. Nine MBA SERS spectra were collected (Figure S3) from five different 100 × 150 $\mu$m areas on three control and three STS treated MBA-AuNF substrates supporting confluent layers of HepG2/C3A.

We used bright-field microscope images of HepG2/C3A cultured on MBA-AuNF to quantify cell rounding after STS and vehicle control treatment (Figure S4). Using ImageJ, we manually highlighted >230 cells in samples exposed to each condition and calculated the roundness of each cell with the ImageJ roundness function.[24]

**Fluorescence Staining.** We seeded HepG2/C3A onto a 96-well plate at 20,000 cells/well, and after 24 h, we treated selected wells with 1 $\mu$m STS or vehicle control for 3 h. We then fixed the cells with 4% formaldehyde for 30 min at room temperature. We washed and permeabilized the cells with 0.1% Triton X in a 2% BSA PBS solution and incubated the sample overnight in 2% BSA PBS solution. After washing, we treated the cells for 2 h with Phalloidin-488 (1:500, Thermofisher) and Hoechst 33342 (1:1000, Invitrogen) in 2% BSA PBS solution.

**Confocal Image Acquistion.** We imaged the stained HepG2/C3A cells with a Cell Voyager 7000 (CV7000, Yokogawa Inc.) and captured confocal fluorescence images using a long working distance 20× objective (Olympus LUCPLFLN 0.45 NA, WD 6.6−7.8 mm) and an Andor Neo sCMOS camera with a 1 × 1 bin. We imaged Hoechst using a 405 nm excitation laser (405 ± 5 nm, 100 mW, Coherent) with a 445/45 nm bandpass emission filter and imaged Phalloidin using a 488 nm excitation laser (488 ± 2 nm, 200 mW, Coherent) with a 525/50 nm bandpass emission filter. Images were captured over a 10 $\mu$m range at 2 $\mu$m Z intervals.

## RESULTS AND DISCUSSION

**Substrate Characterization.** SERS substrates for integrated pHe sensing *in vitro* must be optically transparent, biocompatible, and have a strong SERS response. We utilized thin sheets of AuNF, supported by PDMS, as SERS active substrates to host cell growth and position the AuNF in the cellular microenvironment. Polyurethane nanofibers are


https://doi.org/10.1021/acs.analchem.1c02530
Anal. Chem. 2021, 93, 13844−13851

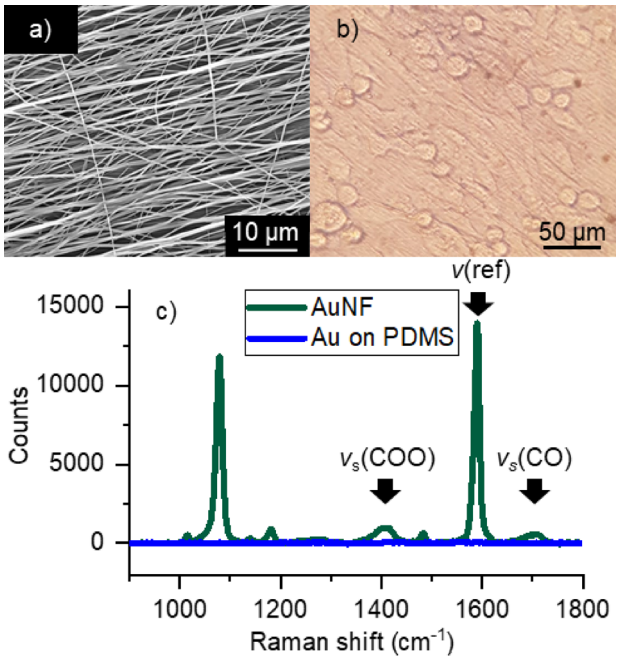


**Figure 1.** (a) SEM image (×2000) of AuNF. (b) HepG2/C3A cells growing on AuNF. (c) Raman spectrum of MBA adsorbed to AuNF and Au on PDMS.

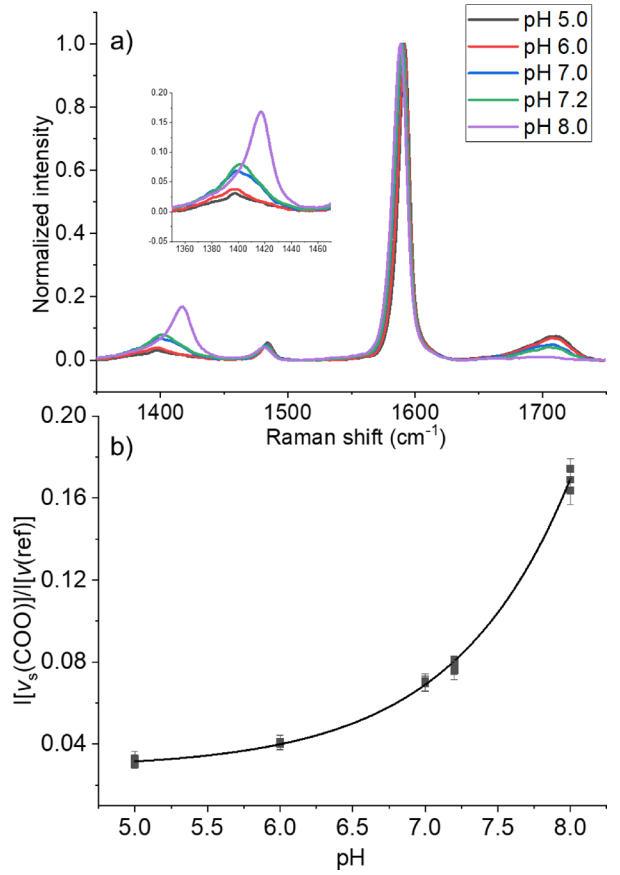


**Figure 2.** (a) SERS spectrum of MBA-AuNF at pH 5−8, normalized to $\nu$(ref). (b) I[$\nu_s$(COO)]/I[$\nu$(ref)] at pH 5−8; three MBA-AuNF samples analyzed at each pH; each data point represents the mean ±SD of 27 spectra collected at different locations on three MBA-AuNF samples.

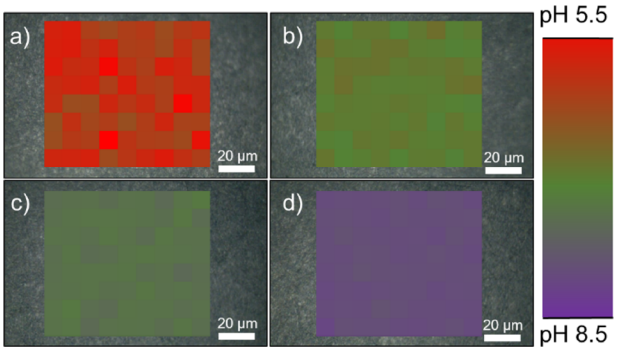


**Figure 3.** A 90 × 80 $\mu$m pH map of the MBA-AuNF surface at (a) pH 6, (b) pH 7, (c) pH 7.4, and (d) pH 8.

**Table 1. Buffer pH Compared to Mean Pixel pH of Maps in Figure 3**

| buffer pH | sensor pH | SD (±) |
|---|---|---|
| 6.00 | 5.93 | 0.25 |
| 7.00 | 6.97 | 0.08 |
| 7.40 | 7.38 | 0.06 |
| 8.00 | 7.99 | 0.04 |

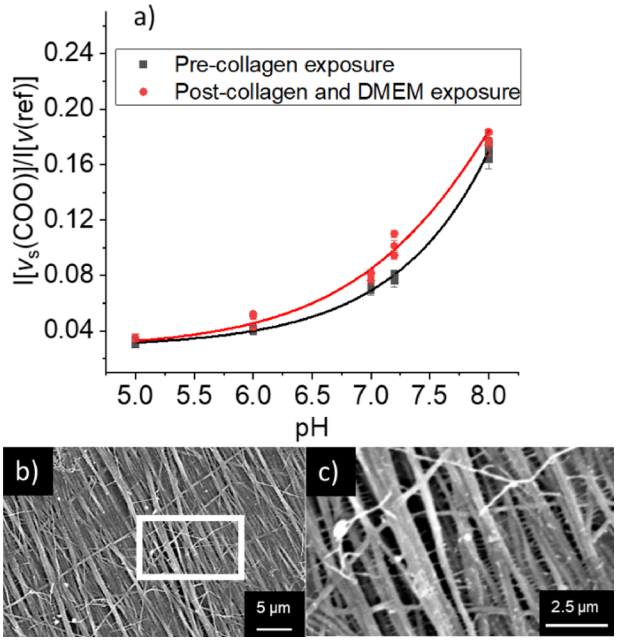


**Figure 4.** (a) MBA-AuNF pH calibration curve pre- and post-preparation for cell culture. (b) SEM image (×3,000) of collagen fibrils bridging the larger MBA-AuNF fibers. (c) A zoomed-in frame of the area highlighted in (b).

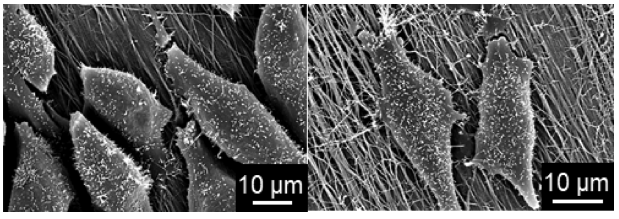


**Figure 5.** SEM images of HepG2/C3A cultured on MBA-AuNF.

biocompatible and well suited to mimicking the cellular microenvironment.[25] The fibers in our AuNF substrate had a



https://doi.org/10.1021/acs.analchem.1c02530
Anal. Chem. 2021, 93, 13844−13851

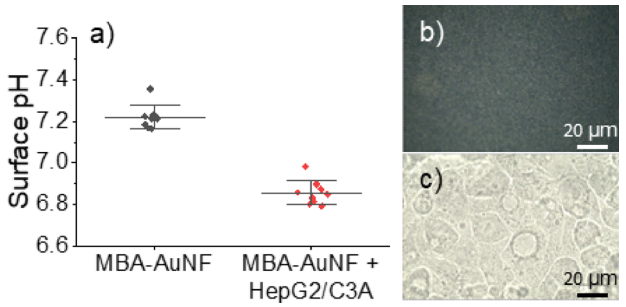


**Figure 6.** (a) MBA-AuNF surface pH with and without HepG2/C3A ($p < 0.01$, two-sample $t$ test). Each data point represents the mean of 9 spectra taken in a 150 × 100 um area (Figure S3); three data points were collected from different areas on three independent MBA-AuNF samples for each condition. (b) A blank MBA-AuNF submerged in the imaging solution. (c) A confluent HepG2/C3A monolayer on the MBA-AuNF surface.

mean diameter of 352 ± 98 nm (Figure 1a). We confirmed the sustained viability and proliferation of HepG2/C3A cells cultured on AuNF by conducting ATP assay CellTiter-Glo at 20 and 63 h and measured a relative increase in the cell population. (Figure S5) Furthermore, our use of PDMS as structural support for fibers ensured that the AuNF film remained thin enough to be transparent, allowing the use of a standard bright-field microscope to monitor cells growing on the AuNF surface (Figure 1b).

The gold-coated nano-fibers in AuNF are SERS active. MBA self-assembled monolayers (SAMs) exhibited a strong SERS effect when adsorbed to AuNF, compared to Au directly sputter-coated onto PDMS in the absence of nanofibers (Figure 1c). This confirms that the gold-coated polyurethane nanofibers facilitate the strong SERS signal observed in Figure 1c.

In Figure 1c, we assigned the Raman peaks at ∼1420 and ∼1700 $cm^{-1}$ to the symmetric carboxylate vibration ($\nu_s$(COO)) and the carbonyl stretch ($\nu_s$(CO)) of MBA. The intensity of $\nu_s$(COO) (I[$\nu_s$(COO)]) and $\nu_s$(CO) (I[$\nu_s$(CO)]) depends on the population of protonated and deprotonated MBA molecules. We assigned the peak at 1590 $cm^{-1}$ to the ring deformation vibration of the MBA aromatic ring ($\nu$(ref)) and used it as a reference against which to normalize MBA spectra for pH sensing.[23] Normalizing the spectra to the intensity of $\nu$(ref) (I[$\nu$(ref)]) allowed us to correlate I[$\nu_s$(COO)] with pH at the MBA-AuNF surface. In this work, we utilized I[$\nu_s$(COO)] for the pH sensor because it increases to 18% of the $\nu$(ref) intensity, while I[$\nu_s$(CO)] only increases to ∼10% of the $\nu$(ref) intensity (Figure 2a). This renders I[$\nu_s$(COO)] more sensitive to pH and a better peak for pH sensing.

**pH Calibration and Sensing with MBA-AuNF.** We collected the SERS spectrum of MBA-AuNF between pH 5 and 8 and normalized each spectrum to the intensity of the $\nu$(ref) peak at 1590 $cm^{-1}$ (Figure 2a). This pH range encompasses the expected pHe of biological tissue.[26] The pH-sensitive $\nu_s$(COO) peak increases in intensity as the pH of the solution and the proportion of deprotonated carboxylate groups at the MBA-AuNF surface increase.

A plot of pH vs the ratio of I[$\nu_s$(COO)]/I[$\nu$(ref)] within a biologically meaningful range is presented in Figure 2b. We fitted a Boltzmann curve to these data with good precision, the use of the Boltzmann curve to describe the pH dependence of I[$\nu_s$(COO)]/I[$\nu$(ref)] has been established by other publications.[23,27] The low standard deviation and dispersion between data points at each pH in Figure 2b confirmed that the I[$\nu_s$(COO)]/I[$\nu$(ref)] ratio was consistent and reproducible across the pH range.

We collected Raman maps at the surface of MBA-AuNF at pH 6, 7, 7.4, and 8 to demonstrate the uniformity of microscale pH measurements with MBA-AuNF (Figure 3). The 90 × 80 $\mu$m Raman maps were created by collecting MBA-AuNF spectra at 10 $\mu$m intervals on the substrate surface. We calculated the pH value for each pixel using the calibration curve in Figure 2b.

Figure 3 highlights the microscale spatial uniformity of pH measurements collected using MBA-AuNF. The standard deviation across the 72 pH pixels was greatest at pH 6, with an SD of ±0.25 (Table 1). We attribute this reduced accuracy at pH 6 to the relatively low intensity of $\nu_s$(COO) at pH 6, ∼4% of I[$\nu$(ref)], and the shallow gradient of the Boltzmann calibration curve in this pH region (Figure 2b). The accuracy of the sensor increased as the pH, and therefore I[$\nu_s$(COO)], increased. MBA-AuNF accuracy improved significantly at pH 7, where pixel pH had a standard deviation of ±0.08 pH units. We anticipate that extracellular pH measurements will lie in the range of pH 6.2−7.4, which encompasses the *in vivo* pHe range of healthy and tumor tissue.[26] The pH sensing capability of MBA-AuNF, together with its spatial addressability and the biocompatible nature of the substrate, makes it an excellent sensor to measure pHe in *in vitro* cellular microenvironments.

**Calibration of MBA-AuNF for pH Sensing in the Cellular Microenvironment.** The pH sensitivity of MBA is influenced by the chemical composition of the immediate environment of the sensor.[9] To support HepG2/C3A cell growth, we treated the MBA-AuNF with collagen solution and submerged the substrate in cell culture media (DMEM). To ensure that pH measurements collected from the cellular microenvironment with MBA-AuNF were accurate, we re-calibrated the sensor post preparation for cell culture, i.e., after incubation in collagen solution and DMEM. Figure 4a presents the calibration curve of MBA-AuNF pre- and post-preparation for cell culture.

We incubated the MBA-AuNF in type 1 collagen solution to create an extracellular environment that promoted cell adhesion. This process created collagen fibrils that coated the MBA-AuNF and formed bridges between adjacent fibers (Figure 4b,c). After coating MBA-AuNF in collagen and incubating with DMEM, the I[$\nu_s$(COO)]/I[$\nu$(ref)] values at pH 6, 7, 7.2, and 8 increased, and the gradient of the calibration curve became steeper between pH 6 and 7.2 (Figure 4a). This had the benefit of increasing the resolution of the sensor in the physiological pH range, increasing the sensitivity of MBA-AuNF to the pHe of cells. Figure 4a demonstrates the importance of calibrating SERS sensors under the same conditions as their intended application. The change in MBA-AuNF pH sensitivity is likely influenced by the collagen layer on the MBA-AuNF surface and the interaction of the MBA SAM with the complex chemical composition of DMEM. We utilize the post-collagen and DMEM exposure calibration curve of MBA-AuNF for all the pH measurements that we present in the following sections.

**Measuring pHe in the Cellular Microenvironment.** We cultured HepG2/C3A on the MBA-AuNF surface and used SERS to measure pHe at the cell−fiber interface. HepG2/C3A is a carcinoma-derived cell line and exhibits increased


https://doi.org/10.1021/acs.analchem.1c02530
Anal. Chem. 2021, 93, 13844−13851

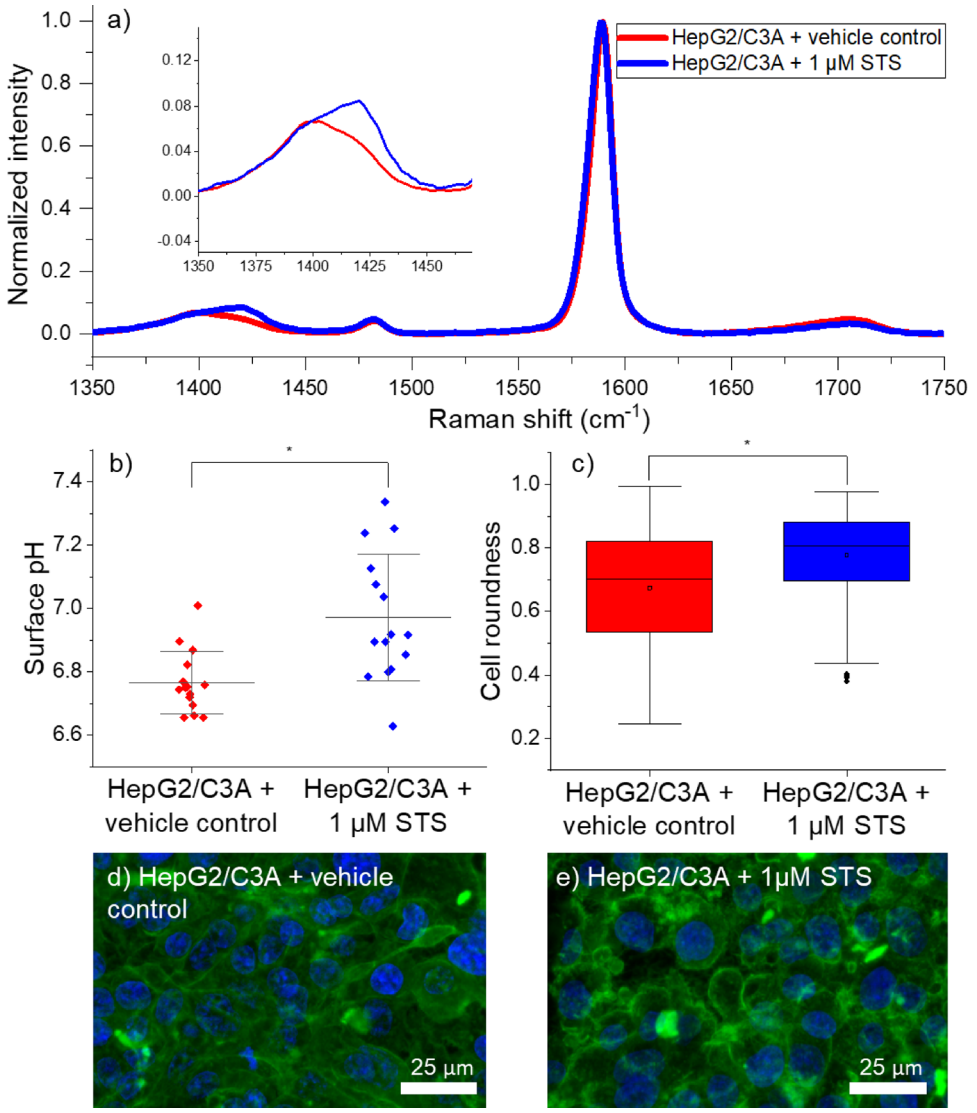


**Figure 7.** (a) Mean SERS spectrum of MBA-AuNF when HepG2/C3A cells on the fiber surface were treated with a control (red) and a 1 $\mu$M STS solution (blue) for 3 h. (b) pHe measured at the cell−fiber interface of HepG2/C3A cells treated with either a control or a 1 $\mu$M STS solution ($p < 0.05$, two-sample $t$ test). Each data point is the mean pH calculated from 9 spectra in an area of 150 × 100 um (Figure S3); five data points were collected from different areas on three independent samples treated with 1 $\mu$M STS or vehicle control for 3 h. (c) Roundness of HepG2/C3A cells cultured on MBA-AuNF and treated with vehicle control or STS solution for 3 h. ($p < 0.05$, two-sample $t$ test). A roundness value approaching 1 indicates cells have a circular morphology. (d) Elongated HepG2/C3A in a 96-well plate, treated with vehicle control (3 h) and stained for F-actin and nuclei. (e) Rounded HepG2/C3A in 96-well plate, treated with 1 $\mu$M STS (3 h) and stained for F-actin and nuclei.

expression and activity of $Na^+/H^+$ exchangers and $H^+$/lactate cotransporters, which contribute to the acidification of the tumor microenvironment *in vivo*.[3]

SEM images confirmed that the HepG2/C3A cells form focal adhesion points with the fiber surface and do not penetrate the dense fiber mesh (Figure 5). HepG2/C3A cells cultured on MBA-AuNF showed a healthy morphology and developed microvilli-like structures on the cell membranes (Figure 5 and Figure S6).

By growing the HepG2/C3A on the surface of collagen-coated MBA-AuNF, we can measure pHe in direct contact with the basolateral cell membrane using SERS (Figure S7). For pHe measurements, we seeded a confluent layer of HepG2/C3A cells onto the MBA-AuNF surface. Figure 6a compares the pH we measured from MBA-AuNF with and without HepG2/C3A cultures on the substrate surface. In the absence of cells (Figure 6b), we recorded a pH of 7.22 ± 0.06 using MBA-AuNF, which is the pH of the PBS imaging solution. We confirmed that the pH of the imaging solution was 7.18 ± 0.01 using a pH electrode. When we cultured HepG2/C3A cells to confluency on the MBA-AuNF (Figure 6c), we calculated a pH of 6.86 ± 0.06 from the SERS spectra collected from the MBA-AuNF surface. This extracellular acidification is driven by proton and lactate secretion, the byproducts of HepG2/C3A cellular metabolism.[3]

By supporting cell growth directly on its surface, MBA-AuNF is sensitive to local variations in pH that cannot be measured in cell cultures using a conventional pH meter. To demonstrate this, we collected pH measurements from ∼1 cm above cells cultured on MBA-AuNF using a conventional pH electrode (Figure S8). We detected no reduction in pH in the presence of HepG2/C3A using this method. This confirmed that the pH measurements in Figure 6 were made possible by


https://doi.org/10.1021/acs.analchem.1c02530
Anal. Chem. 2021, 93, 13844−13851

the proximity and contact of MBA-AuNF with the HepG2/C3A basolateral surface.

**Quantifying the Impact of Staurosporine on the HepG2/C3A pHe Microenvironment.** Staurosporine (STS) is a nonspecific protein kinase inhibitor that induces apoptosis in a wide range of cell lines.[28] Apoptosis plays a pivotal role in the pathogenesis of many diseases. Among these diseases is cancer, where a lack of apoptosis leads to the proliferation of malignant cells upsetting the balance between cell division and cell death. Inducing apoptosis in tumors has been identified as a potential target for treatment.[29] The reverse pH gradient, acidic to basic, between the extracellular and intracellular space of tumor cells is implicated in the lower than expected efficacy of some cancer treatments *in vivo*.[30] To this end, there is a need to understand how the pHe of the tumor microenvironment is influenced by apoptosis.

We investigated the impact of STS treatment on pHe by treating HepG2/C3A, cultured on MBA-AuNF, with 1 $\mu$M STS and a vehicle control solution (0.01% DMSO) for 3 h. At the 3 h time point, we measured a significant increase in cell rounding, a morphological hallmark of apoptosis, in brightfield images of samples treated with 1 $\mu$M STS (Figure 7c). We also observed F-actin reorganization, a key process in the early stages of apoptosis, and cell rounding in fluorescence images of HepG2/C3A treated with 1 $\mu$M STS (Figure 7d,e).[31]

We collected SERS spectra from the cell−fiber interface of HepG2/C3A grown on MBA-AuNF to investigate the impact STS has on the pHe of the cellular microenvironment. Figure 7a presents the mean MBA-AuNF SERS spectrum collected from the basolateral surface of HepG2/C3A cells exposed to the vehicle control and the STS solutions for 3 h. A clear increase in the intensity of $\nu_s$(COO) is visible in the samples treated with STS. This indicates that the pH at the cell−fiber interface is more alkaline after 3 h of STS exposure. Figure 7b presents the pHe measured at five different locations from three vehicle controls and three STS-treated HepG2/C3A cultures. We measured a pHe of 6.75 ± 0.10 in HepG2/C3A cultures treated with the control solution. Following 3 h of exposure to STS, we measured an increase of 0.22 pH units in the mean pHe of HepG2-C3A cells. There was no loss of HepG2/C3A cell coverage after 3 h of STS treatment, and hence this increase in pH is not the result of a reduced cell population. We speculate that this increase in pH is the result of reduced cell−fiber contact during cell rounding, or a decrease in $Na^+/H^+$ exchanger and $H^+$/lactate cotransporter activity, which occurs during the early stages of apoptosis.[1] During apoptosis, cells lose focal adhesion contacts with the extracellular environment, leading to cell rounding. In Figure 7d,e, there is an increase in cell rounding and reorganization of the actin skeleton in STS-treated samples compared to control samples. This reduced contact between fibers and the cell membrane could increase buffer flux to the fiber surface, raising local pH.[31] Hence, using our novel MBA-AuNF sensors, we have correlated changes in cell morphology, which are associated with the early stages of apoptosis, to the pH microenvironment of HepG2/C3A, which is key to tumor pathogenesis.

We have developed a novel SERS substrate by leveraging the nanoscale dimensions of polymer fibers produced by the electrospinning process. While such an easily fabricated substrate with uniform SERS enhancement may have a wide range of applications in vibrational spectroscopy, we have chosen to demonstrate its utility as both a substrate for cell culture and a SERS platform for the measurement of localized pH variations. We have shown that when modified with a pH-responsive reporter (MBA), we can make precise pH measurements in a physiological range (5−8), and when cells are cultured on the surface of MBA-AuNF, we can discriminate local changes in pH as a consequence of metabolic activity. Using this experimental approach, we measured an increase in local pHe, after exposure to protein kinase inhibitor STS, which correlated with morphological changes indicative of apoptosis. MBA-AuNF have great potential as a non-invasive method of collecting biological data, requiring no dye addition or staining. This low-impact sensing methodology could be integrated with microphysiological *in vitro* platforms for non-invasive real-time monitoring of pHe and help build a clearer understanding of the relationship between pHe and disease physiology.

## ■ ASSOCIATED CONTENT

### Supporting Information

The Supporting Information is available free of charge at https://pubs.acs.org/doi/10.1021/acs.analchem.1c02530.

Additional experimental details, cell viability assay, and images of HepG2/C3A on MBA-AuNF (PDF)

## ■ AUTHOR INFORMATION


### Corresponding Author

**Colin J. Campbell** − *EaStCHEM School of Chemistry, University of Edinburgh, The University of Edinburgh, Edinburgh EH9 3FJ, United Kingdom;* orcid.org/0000-0003-1917-6105; Email: colin.campbell@ed.ac.uk

### Authors

**William H. Skinner** − *EaStCHEM School of Chemistry, University of Edinburgh, The University of Edinburgh, Edinburgh EH9 3FJ, United Kingdom;* orcid.org/0000-0002-4307-8356

**Michael Chung** − *School of Engineering, The University of Edinburgh, Edinburgh EH9 3JL, United Kingdom;* orcid.org/0000-0003-0395-3387

**Stephen Mitchell** − *School of Biological Sciences, The University of Edinburgh, Edinburgh EH9 3BF, United Kingdom*

**Asli Akidil** − *Clinical Pharmacology and Safety Sciences, Biopharmaceuticals R&D, AstraZeneca, Cambridge CB4 0WG, United Kingdom*

**Kristin Fabre** − *Innovation Scientist, Baylor College of Medicine, Centre for Space Medicine, Houston, Texas 77030, United States*

**Richard Goodwin** − *Clinical Pharmacology and Safety Sciences, Biopharmaceuticals R&D, AstraZeneca, Cambridge CB4 0WG, United Kingdom*

**Adam A. Stokes** − *School of Engineering, The University of Edinburgh, Edinburgh EH9 3JL, United Kingdom*

**Norbert Radacsi** − *School of Engineering, The University of Edinburgh, Edinburgh EH9 3JL, United Kingdom;* orcid.org/0000-0002-7358-951X

Complete contact information is available at: https://pubs.acs.org/10.1021/acs.analchem.1c02530


### Author Contributions

#These authors contributed equally to this work. The manuscript was written through contributions of all authors.



https://doi.org/10.1021/acs.analchem.1c02530
Anal. Chem. 2021, 93, 13844−13851

W.H.S. did all spectroscopy and cell culture. M.C. did all AuNF fabrication. S.M. fixed and prepared samples for SEM. A.A. provided support and protocols for cell culture of HepG2/C3A cells. R.G., N.R., A.S., A.A., K.F., and C.J.C. all contributed to the experiments and proof reading. All authors have given approval to the final version of the manuscript.

### Notes

The authors declare no competing financial interest.

## ■ ACKNOWLEDGMENTS

WHS and MC were supported by the EPSRC CDT in Intelligent Sensing and Measurement, Grant Number EP /L016753/1. AZ would like to thank Peter Newham for support in initiating the collaboration.

## ■ REFERENCES

(1) Gottlieb, R. A. *Apoptosis* **1996**, *1*, 40−48.
(2) Parks, S. K.; Chiche, J.; Pouysségur, J. *Nat. Rev. Cancer* **2013**, *13*, 611−623.
(3) Cardone, R. A.; Casavola, V.; Reshkin, S. J. *Nat. Rev. Cancer* **2005**, *5*, 786−795.
(4) Simonin, J.; Bille, E.; Crambert, G.; Noel, S.; Dreano, E.; Edwards, A.; Hatton, A.; Pranke, I.; Villeret, B.; Cottart, C.; Vrel, J.; Urbach, V.; Baatallah, N.; Hinzpeter, A.; Golec, A.; Touqui, L.; Nassif, X.; Galietta, L. J. V.; Planelles, G.; Sallenave, J.; Edelman, A.; Sermet-Gaudelus, I. *Sci. Rep.* **2019**, *9*, 6516.
(5) Gillies, R. J.; Raghunand, N.; Karczmar, G. S.; Bhujwalla, Z. M. *J. Magn. Reson. Imaging* **2002**, *16*, 430−450.
(6) Chen, Y. *Anal. Biochem.* **2021**, *612*, 113900.
(7) Yang, Y.; Xia, M.; Zhao, H.; Zhang, S.; Zhang, X. *ACS Sens* **2018**, *3*, 2278−2285.
(8) Zhao, W.; Schafer, S.; Choi, J.; Yamanaka, Y. J.; Lombardi, M. L.; Bose, S.; Carlson, A. L.; Phillips, J. A.; Teo, W.; Droujinine, I. A.; Cui, C. H.; Jain, R. K.; Lammerding, J.; Love, J. C.; Lin, C. P.; Sarkar, D.; Karnik, R.; Karp, J. M. *Nat. Nanotechnol.* **2011**, *6*, 524−531.
(9) Sun, F.; Zhang, P.; Bai, T.; David Galvan, D.; Hung, H.-C.; Zhou, N.; Jiang, S.; Yu, Q. *Biosens* **2015**, *73*, 202−207.
(10) Xu, M.; Ma, X.; Wei, T.; Lu, Z.-X.; Ren, B. *Anal. Chem.* **2018**, *90*, 13922−13928.
(11) Fleischmann, M.; Hendra, P. J.; McQuillan, A. J. *Chem. Phys. Lett.* **1974**, *26*, 163−166.
(12) Lee, S.; Chon, H.; Lee, J.; Ko, J.; Chung, B. H.; Lim, D. W.; Choo, J. *Biosens* **2014**, *51*, 238−243.
(13) Qian, X. M.; Nie, S. M. *Chem. Soc. Rev.* **2008**, *37*, 912−920.
(14) Reneker, D. H.; Yarin, A. L. *Polymer* **2008**, *49*, 2387−2425.
(15) Kasani, S.; Curtin, K.; Wu, N. *NANO* **2019**, *8*, 2065−2089.
(16) Yang, T.; Ma, J.; Zhen, S. J.; Huang, C. Z. *ACS Appl. Mater. Interfaces* **2016**, *8*, 14802−14811.
(17) Yu, M.; Dong, R.-H.; Yan, X.; Yu, G.-F.; You, M.-H.; Ning, X.; Long, Y.-Z. *Macromol. Mater. Eng.* **2017**, *302*, 1700002.
(18) Keirouz, A.; Chung, M.; Kwon, J.; Fortunato, G.; Radacsi, N. *Wiley Interdiscip. Rev. Nanomed. Nanobiotechnol.* **2020**, *12*, No. e1626.
(19) Kitsara, M.; Agbulut, O.; Kontziampasis, D.; Chen, Y.; Menasché, P. *Acta Biomater.* **2017**, *48*, 20−40.
(20) Grasl, C.; Bergmeister, H.; Stoiber, M.; Schima, H.; Weigel, G. *J. Biomed. Mater. Res.* **2010**, *93A*, 716−723.
(21) Jia, L.; Prabhakaran, M. P.; Qin, X.; Ramakrishna, S. *J. Biomater. Appl.* **2014**, *29*, 364−377.
(22) Bao, Y.; Lai, C.; Zhu, Z.; Fong, H.; Jiang, C. *RSC Adv.* **2013**, *3*, 8998−9004.
(23) Jaworska, A.; Jamieson, L. E.; Malek, K.; Campbell, C. J.; Choo, J.; Chlopicki, S.; Baranska, M. *Analyst* **2015**, *140*, 2321−2329.
(24) Schneider, C. A.; Rasband, W. S.; Eliceiri, K. W. *Nat. Methods* **2012**, *9*, 671−675.
(25) Lee, K. H.; Kwon, G. H.; Shin, S. J.; Baek, J.-Y.; Han, D. K.; Park, Y.; Lee, S. H. *J. Biomed. Mater. Res.* **2009**, *90A*, 619−628.
(26) Kraus, M.; Wolf, B. *Tumor Biol.* **1996**, *17*, 133−154.
(27) Wang, F.; Widejko, R. G.; Yang, Z.; Nguyen, K. T.; Chen, H.; Fernando, L. P.; Christensen, K. A.; Anker, J. N. *Anal. Chem.* **2012**, *84*, 8013−8019.
(28) Belmokhtar, C. A.; Hillion, J.; Ségal-Bendirdjian, E. *Oncogene* **2001**, *20*, 3354−3362.
(29) Wong, R. S. Y. *J. Exp. Clin. Cancer Res.* **2011**, *30*, 87.
(30) Wojtkowiak, J. W.; Verduzco, D.; Schramm, K. J.; Gillies, R. J. *Mol. Pharmaceutics* **2011**, *8*, 2032−2038.
(31) Desouza, M.; Gunning, P. W.; Stehn, J. R. *BioArchitecture* **2012**, *2*, 75−87.


https://doi.org/10.1021/acs.analchem.1c02530
*Anal. Chem.* 2021, 93, 13844−13851